Journal of Biomechanics 87 (2019) 1–12

Contents lists available at ScienceDirect

Journal of Biomechanics

journal homepage: www.elsevier.com/locate/jbiomech
www.JBiomech.com

Review

Calcifications in atherosclerotic plaques and impact on plaque biomechanics

Hilary E. Barrett [a,*], Kim Van der Heiden [a], Eric Farrell [b], Frank J.H. Gijsen [a], Ali C. Akyildiz [a]

[a] Department of Biomedical Engineering, Thoraxcenter, Erasmus Medical Center, Rotterdam, The Netherlands
[b] Department of Oral and Maxillofacial Surgery, Erasmus Medical Center, Rotterdam, The Netherlands

ARTICLE INFO

Article history:
Accepted 9 March 2019

Keywords:
Plaque rupture
Microcalcification
Macrocalcification
Mechanical properties

ABSTRACT

The catastrophic mechanical rupture of an atherosclerotic plaque is the underlying cause of the majority of cardiovascular events. The infestation of vascular calcification in the plaques creates a mechanically complex tissue composite. Local stress concentrations and plaque tissue strength properties are the governing parameters required to predict plaque ruptures. Advanced imaging techniques have permitted insight into fundamental mechanisms driving the initiating inflammatory-driven vascular calcification of the diseased intima at the (sub-) micron scale and up to the macroscale. Clinical studies have potentiated the biomechanical relevance of calcification through the derivation of links between local plaque rupture and specific macrocalcification geometrical features. The clinical implications of the data presented in this review indicate that the combination of imaging, experimental testing, and computational modelling efforts are crucial to predict the rupture risk for atherosclerotic plaques. Specialised experimental tests and modelling efforts have further enhanced the knowledge base for calcified plaque tissue mechanical properties. However, capturing the temporal instability and rupture causality in the plaque fibrous caps remains elusive. Is it necessary to move our experimental efforts down in scale towards the fundamental (sub-) micron scales in order to interpret the true mechanical behaviour of calcified plaque tissue interactions that is presented on a macroscale in the clinic and to further optimally assess calcified plaques in the context of biomechanical modelling.

Contents

* Corresponding author at: Department of Biomedical Engineering, Thoraxcenter, Erasmus Medical Center Ee2341, P.O. Box 2040, 3000 CA Rotterdam, the Netherlands.
E-mail address: h.barrett@erasmusmc.nl (H.E. Barrett).

https://doi.org/10.1016/j.jbiomech.2019.03.005
0021-9290/

1. Introduction

Atherosclerotic plaque rupture is the underlying cause of the majority of acute myocardial infarction (Jia et al., 2013; Yahagi et al., 2015) and stroke events (Spagnoli et al., 2004). Rupture prone plaques are characterised by their complex, heterogeneous composition, which can include a necrotic core, fibrous cap, inflammatory cells and the presence of calcification (Virmani et al., 2006). Physiologically induced plaque rupture is fundamentally a mechanical event which ensues if the local stress levels exceed the local tissue strength (Richardson, 2002; Cheng et al., 1993). As both plaque stresses and strength strongly depend on plaque composition, calcifications are likely to have a determining role in the plaque's overall mechanical behaviour.

Tackling the growing epidemic regarding calcification in plaque tissue remains a critical clinical challenge. Acute cardio- and cerebrovascular events are strongly associated with vascular calcification. For coronary vasculature, the overall coronary artery calcium score, detected with non-invasive imaging, provides incremental value over traditional risk scores to identify high risk cardiovascular disease patients (Criqui et al., 2017; Greenland et al., 2018). Moreover, it has been advocated that imaging structural features of calcifications in coronary arteries using intravascular ultrasound (IVUS) (van der Giessen et al., 2011) or optical coherence tomography (OCT) (Tearney et al., 2012) and in carotid arteries using computed tomography (CT) (Yang et al., 2018) can be relevant for predicting plaque rupture. Specifically, studies have evidenced that superficial 'spotty' calcifications may induce plaque rupture (Sakaguchi et al., 2016; Nerlekar et al., 2018). In carotid arteries, although a meta-analysis reported less calcification for the clinically symptomatic plaques than the asymptomatic ones (Kwee, 2010), histomorphometric analyses associated ulcerations with superficial, thin calcifications (Yang et al., 2018) and the presence of small ruptures, referred to as fissures, to calcification presence (Daemen et al., 2016). Despite this wealth of clinical data, the fundamental role of calcification on plaque rupture is still largely unclear.

In order to solve this biomechanical challenge, it is necessary to evaluate the current clinical evidence in parallel with mechanical experiments and computational simulations which together can provide a means to contextualise the fundamental mechanics driving the fate of the calcified plaque tissue and calcification for plaque rupture. It is requisite to understand the intricate interplay between the calcification morphology and associated plaque tissue mechanics at multiple length scales. The co-existence of both macrocalcifications and microcalcification particles in cardiovascular events further creates juxtaposition in the current biomechanical plaque stability paradigm (Gupta et al., 2015).

As illustrated in Fig. 1, this review aims to provide an overview of the current knowledge base regarding calcification in terms of structural evolution (Section 2), methods of calcification detection in the clinical setting (Section 3), mechanical influence of calcification in plaque tissue derived from specialised *in vitro* experiments (Section 4), computational modelling efforts which tackle the impact of calcification on plaque stresses (Section 5) and a discussion of the future work that can enhance the mechanical understanding and the possible implementation of clinic parameters for plaque rupture prediction (Section 6).

2. Calcification mechanisms

Vascular calcification forms in the intima of inflamed atherosclerotic arteries. The initiating phases of the calcification formation at the fundamental submicron and micron length scales are illustrated in (Fig. 1: Phase). Fig. 2 demonstrates the three mechanisms; osteogenic trans-differentiation, apoptosis and calcifying extracellular release, which are advocated as playing a role in calcification initiation (Shanahan, 2007; Raggi et al., 2018). A multitude of different resident and circulating cells are subjected to such processes, including endothelial progenitor cells, mesenchymal stem cells, macrophages and vascular smooth muscle progenitor cells (VSMC) (Johnson et al., 2006; Leszczynska et al., 2016; Boström et al., 2016). In this regard, the process possibly mimics the developmental process of endochondral ossification which is responsible for forming long bones (Johnson et al., 2006). Endothelial progenitor cells are susceptible to bone induction and endothelial markers are expressed in calcified cells indicating a role for endothelial cells overlying the plaque in superficial microcalcification formation (Yao et al., 2013; Sánchez-Duffhues et al., 2015; Guihard et al., 2016). Animal studies have also demonstrated that both the atherosclerotic environment itself and stem/progenitor cells derived from atherosclerotic ($ApoE^{-/-}$ mice) animals contribute to ectopic calcification (Leszczynska et al., 2016). VSMCs undergo osteogenic transition to calcifying VSMC in the presence of pathologically stressed environments, like in the plaque, and adapt the same mineralisation processes of osteoblasts while maintaining their own identity (Hunt et al., 2002). Microcalcification particles are fundamentally derived from the expression of bone regulating proteins, alkaline phosphatase and bone-like cells (osteoblasts, osteocytes and osteoclasts; Boulanger et al., 2017; Menini et al., 2013; Aikawa et al., 2007; Hunt et al., 2002).

Activated macrophages secrete proinflammatory cytokines inducing VSMC apoptosis, and calcifying extracellular vesicles (cEV) are released by the elevated calcium derived from the apoptotic bodies providing nucleation sites for initiating microcalcification in the plaque (Shanahan, 2007; Raggi et al., 2018). The cEVs directly meditate calcification through their surface-based calcium binding complexes and have a diameter in the range of 30–400 nm (Bakhshian Nik et al., 2017). The microcalcification particles (Fig. 1: phase) are developed from the four step process including cEV accumulation, aggregation, fusion of cEV membranes and finally mineralisation (Hutcheson et al., 2016). At the mineralisation stage, amorphous calcium phosphate transforms into mature crystalline hydroxyapatite 'microcalcification' particles, portraying spherical and needle like morphology types, typically 0.5–15 μm large (Perrotta and Perri, 2017).

With atherosclerotic disease progression, microcalcification particles coalesce and grow within plaque's necrotic core, fibrous cap and outer bordering medial tissue matrix where localisation is largely regulated by local collagen fiber directionality

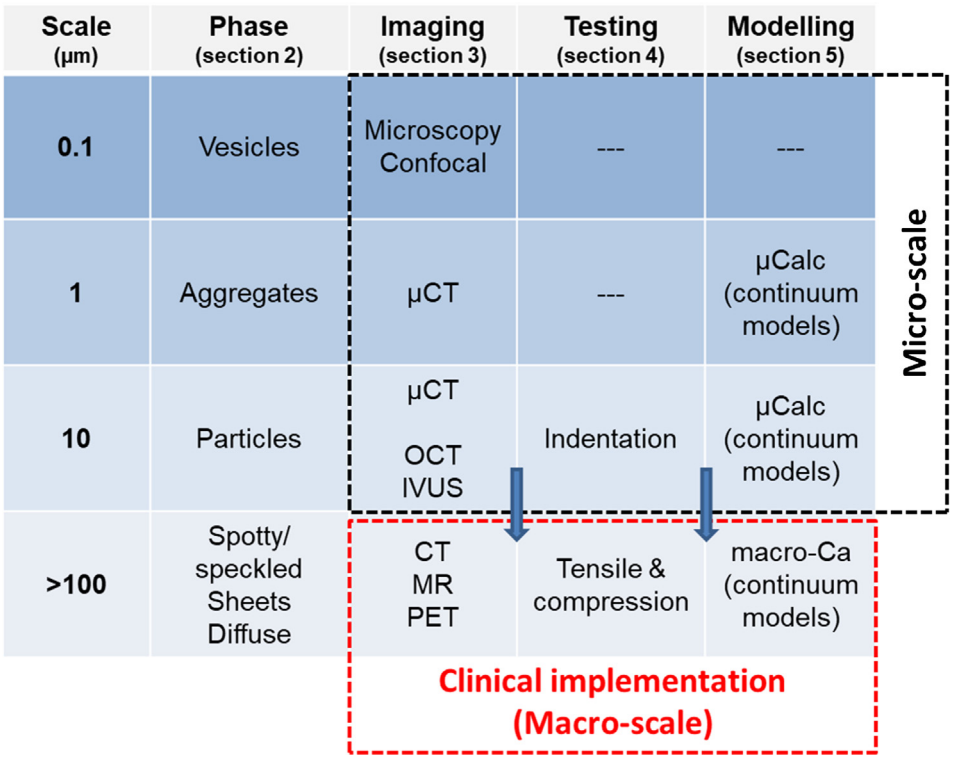

Fig. 1. Overview of the sections of the paper, incorporating the development phase, imaging, testing and modelling of calcification at the fundamental micron scale and working towards the clinical macroscale.

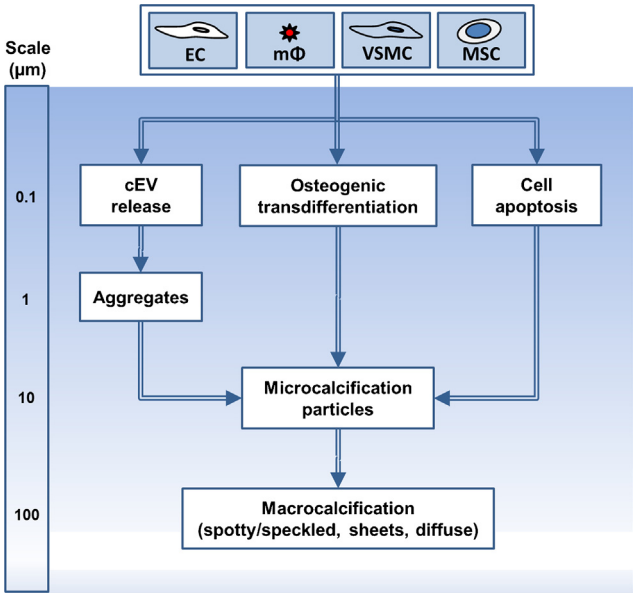

Fig. 2. Mechanisms involved in calcification development. Endothelial progenitor cells (EC), macrophages (mϕ), vascular smooth muscle cells (VSMC) and mesenchymal stem cells (MSC). Calcifying extracellular vesicles (cEV), apoptotic cells and osteogenic transdifferentiation result in microcalcification particles. The continuous coalescence of microcalcification particles transforms into macroscopic calcification formations of distinct geometries.

(Hutcheson et al., 2016; Stary, 2000). Microcalcification particles detected in the fibrous cap are no larger than 50 μm in diameter (Kelly-Arnold et al., 2013). Importantly, collagen fiber orientation can differ depending on local plaque eccentricity as evidenced with MR-based diffusion tensor imaging (Akyildiz et al., 2017). Concentric plaques, predominantly have longitudinally oriented collagen fibers at the lumen while circumferentially oriented fibers are more abundant abluminally. Thus, depending on local calcification developments a multitude of calcification-fibrous tissue interactions can also exist which is mechanically important.

Tracking microcalcification progression over time, both *in vitro* using cell cultured collagen scaffolds (Hutcheson et al., 2016) and *in vivo* in ApoE$^{-/-}$ mice (New et al., 2013), strongly advocates that microcalcification particles coalesce, forming fragments and larger masses of compact calcification. Notably, calcification formation is a dynamic process and during plaque progression to the advanced fibro-calcific plaque type, calcifications in the order of micrometer and millimetre scales can co-exist (Burke et al., 2001). The most advanced calcification formations detected in plaques have resembled osteoid metaplasia with mature calcified matrix, a lamellar structure and even bone marrow (Herisson et al., 2011; Hunt et al., 2002).

3. Calcification imaging

The knowledge base concerning the pathological development of ectopic vascular calcification provides a 'ground-truth' basis for classifying calcification utilising clinical imaging techniques. In the early disease phase vesicles and microcalcification particles are the primary targets while in the more advanced phase larger macrocalcification are present in coexistence with these vesicles and particles. Fig. 3 illustrates the three distinct macrocalcification geometries that evolve with plaque progression: (1) speckled; spotty calcification flecks (~50 μm), (2) sheet-like fragments; linear or wide single focus of calcium (>2 mm in diameter) and (3) diffuse; segments of continuous calcification (≥5 mm) (Burke et al., 2001; Friedrich et al., 1994). It is imperative for plaque rupture assessment to incorporate the (1) full calcification scale range; from initiating vesicles to micron scale particles and millimetre

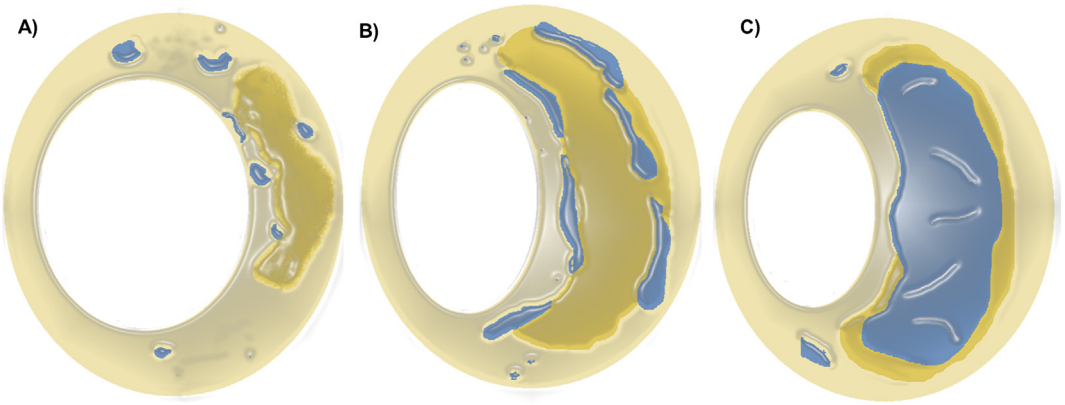

Fig. 3. Macrocalcification geometry classification on clinical imaging (A) spotty/speckled: spotty calcification flecks (~50 μm), (B) sheet-like fragments: linear or wide single focus of calcium (>2 mm in diameter) and (C) diffuse: segments of continuous calcification (≥5 mm).

scale macrocalcification and (2) calcification geometry delineation; detecting the diverging morphology types. This section will examine the calcification features that can be acquired utilising clinical imaging modalities (non-invasive/invasive) and the features that remain confined to the preclinical setting (Fig. 1: imaging).

3.1. Non-invasive clinical imaging

In terms of non-invasive imaging, clinical-computed tomography (CT) can detect vascular macrocalcifications in 3D space with an in-plane spatial resolution in the submillimetre range (~400 μm) (Nikolaou et al., 2004). Clinical-CT is regarded as the gold standard for imaging calcifications, as they strongly attenuate the emitted X-rays thereby creating high contrast from surrounding tissues. However, this high attenuation can cause calcification spill-over effects (blooming) into surrounding voxels of lower intensity. (Sarwar et al., 2008). Blooming artefact of macrocalcifications thus can mask calcification fragments in close proximity. The fragments and larger calcification can show up in the CT-scan as one unified mass (Fig. 4), which is a major concern for biomechanical assessment, as the coexistence of a diffuse macrocalcification versus multiple speckled calcifications in close proximity can have a significantly different impact on plaque tissue stress distribution.

Additionally, blooming artefact negatively affects the accurate delineation of surrounding non-calcified plaque components. In this regard, magnetic resonance imaging (MRI) is superior to clinical-CT and is capable of discriminating multiple components including lipid core, fibrous tissue and calcifications (van Wijk

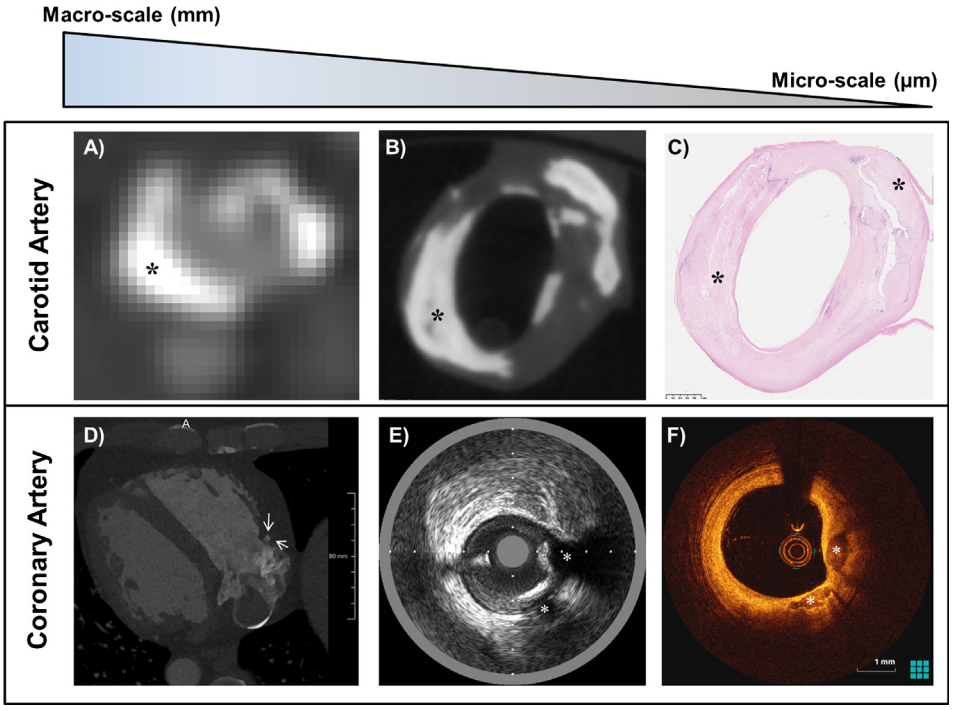

Fig. 4. Illustration of non-invasive, invasive and preclinical image scan results of one carotid artery (top row) and one coronary artery plaque (bottom row) from the macro-scale down to the micro-scale. Non-invasive imaging of heavily calcified carotid plaque with (A) Clinical computed tomography, (B) preclinical micro-computed tomography and (C) corresponding decalcified hematoxylin and eosin histology cross-section. Invasive catheter based imaging of superficial spotty calcification in the right coronary artery detected on (D) contrast-enhanced computed tomography angiography, (E) intravascular ultrasound and (F) optical coherence tomography (example patient scan images were obtained with written informed consent from each participant undergoing the diagnostic imaging and surgical procedure and study protocols were approved by the institutional Medical Ethical Committee).

et al., 2015). The 3D geometric information can be generated from multi-sequential protocols, usually including T1-, T2- and proton density-weighted sequences and time of flight. The typical in-plane resolution for a clinical 3 Tesla scanner is 500 μm (van Wijk et al., 2015). The calcification can be discriminated from the surrounding plaque tissue as a hypointense signal area, visible on all four sequences (Den Hartog et al., 2013). MRI can detect calcification with high sensitivity and specificity (Puppini et al., 2006); however, can underestimate macrocalcification areas due to the partial volume artefact (Saam et al., 2007).

The application of positron emission tomography (PET) imaging in cardiovascular field has potentiated advancement towards the detection of microcalcification particles (Vesey et al., 2017; Dweck et al., 2016). Early stage microcalcification particles can be identified through 18F-sodium fluoride radiotracer uptake in coronaries and carotids, which is reflected as a signal intensity of the indirect gamma-ray emittance. The uptake mechanism is based on fluoride ion exchange with a hydroxyl group present on the hydroxyapatite particles' surface and thus forming fluor-apatite (Irkle et al., 2015). It is imperative to mention that poor spatial resolution of clinical-PET remains a concern regarding the localisation of signal detection (typical in-plane resolution 3–4 mm) (Doris and Newby, 2016). Notwithstanding, a hybrid molecular-functional imaging approach coupling PET with CT or MRI can greatly enhance our understanding about the influence of calcifications and other components on the fibrous plaque tissue due to the additional geometrical information of PET/MR (Robson et al., 2018).

3.2. Invasive clinical imaging

Moving down in size scale (Fig. 1: imaging), intravascular ultrasound (IVUS) imaging of the coronaries identifies calcification as bright hyperechoic (white) regions, with sharp-edged borders due to its strong reflectance of the high frequency sound waves (axial resolution 40–100 μm and lateral resolution 200–300 μm) (Jian et al., 2017). IVUS can detect 50% more calcification than contrast enhanced clinical-CT, specifically capturing the smaller calcifications (van Der Giessen et al., 2011). For heavily calcified vessels, IVUS suffers from acoustic shadowing and fails to penetrate the macrocalcification deposits. Thus, volume and radial thickness measurements can be unreliable in such vessels.

Optical coherence tomography (OCT) is an alternative modality, that uses near-infrared light and has the most superior sensitivity and specificity with an in-plane resolution of ~10 μm (Fujimoto, 2003). While this technique is confined juxtaluminal region, due to constraints in the penetration depth (~2–3 mm) (Fujimoto, 2003), it can resolve accurate delineation of superficial calcification (Mehenna et al., 2013) and surrounding fibrous tissue (Fig. 4). The sharp delineation of the calcification borders can be attributed to the near-infrared backscatter of light measurement which denotes calcification as signal-poor region. OCT assessment of acute coronary syndrome patients revealed a higher abundancy of spotty calcifications in the ruptured vessels, which were specifically localised close to the luminal surface and plaque rupture site (Sakaguchi et al., 2016) and positively correlated with cap thinning (Kataoka et al., 2014).

3.3. Preclinical imaging

Notably, the aforementioned clinical imaging modalities exclude micrometre scale calcification particles (0.5–15 μm) due to the resolution restrictions. In lower resolution CT scanners, clusters of particles are detected as single calcification particles, providing misleading plaque stress distribution (Vengrenyuk et al., 2008). Thus, pre-clinical micro-CT with high spatial resolution of 2 μm (reconstructed) remains the only technique to resolve accurate 3D geometries including spatial distribution, clustering and abundancy of micron scale particles (>5 μm) embedded in fibrous tissue (Kelly-Arnold et al., 2013). Coronary plaques contain hundreds to thousands of microcalcification particles less than 50 μm in the fibrous cap. Technological advancements have further improved the capability of preclinical CT scanners to now achieve spatial resolution in the nanoscale range. Nano-CT scanners are capable of visualising and reconstructing tissue features of ~400 nm and the typical sample size for a single nano-CT scan is approximately 1 mm (Cnudde et al., 2006). This provides potential for the detection of initiating vesicles and the smallest calcification particles of 0.5 μm. At this scale, the advent use of nano-analytical microscopy (Fig. 1: imaging) techniques coupled with mineralogical characterisation has greatly advanced the understanding regarding cellular and molecular mechanisms involved in vascular calcification, which originate from nanoscale cells transitioning to microscopic particles (Perrotta and Perri, 2017; Hutcheson et al., 2016; Bertazzo et al., 2013).

3.4. Summary

The non-invasive imaging techniques are widely used to screen for calcification in acute symptomatic and asymptomatic patients of all vascular territories. While the specific geometrical features of speckles or sheets cannot be delineated if in close proximity to the lumen due to resolution restrictions, the overall detection of calcification provides instrumental value to gauge the disease burden status. Mineralised vesicles and microcalcification particles may be detected if in high concentration presenting brighter spots on CT, but not reaching the accepted Hounsfield density threshold of 130HU for calcium, thereby proving difficult to delineate using the current Agatston scoring (Agatston et al., 1990). Although these mineralised vesicles and micro-particles cannot be imaged individually, their presence detected by PET signal due to high sensitivity detectors is of expected value for mechanical assessment. Detecting calcification features accurately on invasive imaging is superior to noninvasive clinical-CT and MRI, ultimately due to higher resolution capabilities, which might enhance the biomechanical destabilisation understanding induced by calcification. Overall, OCT is a promising modality for superficial calcification detection providing means to evaluate the morphological features of the calcification inclusions as illustrated in Fig. 4.

4. Calcification & calcified plaque tissue mechanical properties

To evaluate how calcification geometrical features influence the biomechanical behaviour of the plaque tissue, it is important to characterise the mechanical properties using ex-vivo experimental tests. Traditional macroscale experimental approaches, including uniaxial tension and compression have been performed on excised human calcified plaque tissue material. The majority of mechanical tests performed were on tissue level at the macroscopic scale (Fig. 1; testing), where the mechanical properties obtained are determined by the combined influence of calcification and surrounding plaque tissue.

The reported mechanical results, including stiffness and ultimate failure properties, are summarised in Table 1. In the case where stiffness was not reported, we have calculated the values from the reported stress–strain curves using their digitised plots for comparison purposes in this review.

4.1. Indentation experiments

Indentation tests have been utilised to determine local properties of partially calcified fibrous tissue, defined as predominantly

Table 1
Summary of the mechanical properties of human arterial plaques containing calcification derived from *ex vivo* mechanical experiments.

			Mechanical test			Calcification		Properties		
Author	Vessel	n	Test	Direction	Test conditions	Modality	Classification	Stiffness	Failure stress (MPa)	Failure stretch
(Salunke et al., 2001)	Iliac	5	Unconfined compression	Radial	Relaxation 25% strain 600 s	Histology	Calcified	Max. 2.49 MPa	–	–
(Cahalane et al., 2018)	Carotid Femoral	10 7	Indentation	Axial	Indentation depth 2 μm 0.05/s	Micro-CT	Calcification Geometry	Moderate 17.64 ± 6.63 GPa High 25.26 ± 6.18 GPa Low 8.47 ± 8.84 GPa	–	–
(Ebenstein et al., 2009)	Carotid	10	Indentation	Radial	600 μN hold for 10 s	Fourier transform infrared	Partially calcified tissue Calcification	2.1 ± 5.4 MPa 0.69 ± 2.3 GPa	–	–
(Maher et al., 2009)	Carotid	8	Unconfined compression	Radial	1% strain/s	Grey scale median	Calcified	0.1–4 MPa (~20% strain)	–	–
(Maher et al., 2011)	Carotid	8	Cyclic compression	Radial	5%strain/s	Grey scale median	Calcified	a 68.5 ± 49.5 kPa C. 13.3 ± 10.04 kPa	–	–
(Holzapfel et al., 2004)	Iliac	4	Tensile	Circumference Axial	0.016 mm/s	hr MRI and Histology	Calcification	12.6 ± 4.7 MPa	0.179 ± 0.056	1.02 ± 0.005
(Cunnane et al., 2015)	Femoral	15	Planar tension	Circumferential	30% gauge length/s	Fourier transform infrared	Low Moderate High	0.89 ± 0.51 MPa (>40% strain)	0.3 ± 0.01 0.43 ± 0.11 0.16 ± 0.04	2.16 ± 0.09 1.75 ± 0.19 1.55 ± 0.21
(Lawlor et al., 2011)	Carotid	14	Planar tension	Circumferential	0.5 mm/s	Grey scale median	Hard	–	0.342 ± 0.16	0.49 ± 0.09
(Mulvihill et al., 2013)	Carotid	23	Planar tension	Circumferential	30% of gauge length /s	Fourier transform infrared	Calcifed:Lipid > 1 Calcifed:Lipid < 1	0.44 ± 0.26 MPa (>40% strain)	0.618 ± 0.23	1.927 ± 0.26 1.631 ± 0.17
(Barrett et al., 2017)	Carotid	17	Planar tension	Circumferential	30% of gauge length /s	Micro-CT	Speckled Diffuse Concentric	0.019–0.46 MPa at 20% strain	0.47 ± 0.08 0.27 ± 0.09 0.52 ± 0.097	2.00 ± 0.07 1.74 ± 0.2 2.42 ± 0.3

fibrous tissue with local calcifications that are too small to isolate, and whole calcifications dissected from human carotid bifurcation plaque (fresh and frozen) (Ebenstein et al., 2009). The Young's modulus (E) for partially calcified fibrous tissue was 2.1 ± 5.4 MPa. Though, a large range has been detected reaching a maximum stiffness of 43 MPa for the partially calcified fibrous tissue. The reported mean Young's modulus of isolated calcification particles was 0.69 ± 2.3 GPa with a maximum of 21 GPa. Nanoindentation experiments have further identified the Young's modulus of specific calcification geometries in carotid and femoral plaques (Cahalane et al., 2018). Speckled and spotty calcifications demonstrated the lowest stiffness properties of 8.47 ± 8.84 GPa. Sheet-like calcifications incorporated both moderate stiffness (17.64 ± 6.63 GPa) and high stiffness (25.26 ± 6.18 GPa), and diffuse calcification properties fell in the high stiffness range (Cahalane et al., 2018). No significant differences were identified between the of the carotid and femoral calcifications.

4.2. Unconfined compression

Iliac plaques, histologically classified with a predominantly calcified necrotic core, were subjected to unconfined compression testing characterising the non-linear stiffening behaviour of the tissue (Salunke et al., 2001). The testing was performed in radial direction on fresh calcified common, internal and external carotid plaque tissue segments classified by duplex ultrasound (calcified, mixed and echolucent). The calcified segments were 1.5–2 times stiffer than mixed ones and twice the echolucent type. This test identified a large degree of variability within the calcified segments, which underscores the structural heterogeneity in plaque with one extremely stiff plaque of 12.2 MPa not capable of deforming to 20% strain (Salunke et al., 2001). The inelastic mechanical properties of calcified carotid plaque tissue segments were also tested under cyclic radial compression. Comparison of the calcified, mixed and echolucent types revealed that calcified plaques had the stiffest response, and the plastic deformation linearly increased with an increase in peak applied strain and the magnitude of permanent deformation upon unloading did not differ (Maher et al., 2011).

4.3. Tension

Quasi-static uniaxial tensile tests on histologically classified rectangular strips of calcified intimal plaque tissue from iliac arteries in both axial and circumferential directions identified a linear stiffness response (Holzapfel et al., 2004). Also planar tension experiments have been applied to femoral and carotid plaque samples (Barrett et al., 2016; Cunnane et al., 2015; Mulvihill et al., 2013; Lawlor et al., 2011). These tests differ from tensile tests whereby a sample width to length ratio of 4:1 facilitates testing whole plaques samples in the circumferential direction. Heavily calcified carotid plaques with diffuse calcification varied in stiffness from 0.019 MPa to 0.46 MPa at 20% strain (Barrett et al., 2016). The stiffness properties of calcified femoral plaque tissue were significantly higher than carotid [0.89 ± 0.51 MPa vs. 0.44 ± 0.26 MPa] due to higher amount of calcification (Cunnane et al., 2016). Notably, these carotid and femoral stiffness values were measured in the high stretch domain (>1.4) emulating the stiffness at experienced during endovascular deployment.

4.4. Failure properties

An inverse relationship exists between the degree of calcification and a plaque's capacity to stretch (Barrett et al., 2016; Cunnane et al., 2015; Mulvihill et al., 2013). Typical circumferential failure stretch of whole femoral plaques decrease from 2.16 ± 0.09 in lightly calcified to 1.75 ± 0.19 in moderately calcified and to 1.55 ± 0.21 in heavily calcified samples. Heavily calcified carotid plaques with diffuse calcification and a calcified volume fraction of 26.63 ± 8.65% possess the lowest stretch at failure with a mean value of 1.74 ± 0.2, in line with moderately calcified femoral plaques. Interestingly, plaques with sheet-like calcification have the largest stretch capacity before failing (2.42 ± 0.3) due to the shearing (sliding) mechanism of the fibrous tissue parallel to the calcification sheets whereas for diffuse calcified plaques stretch properties depend on the remaining non-calcified tissue stretch (Barrett et al., 2017).

Calcified iliac plaques have circumferential failure stress of 0.255 ± 0.08 MPa and an axial failure stress of 0.468 ± 0.1 MPa. In general, the reported failure stress of 0.49 ± 0.23 MPa for carotid plaques are higher than femoral plaques (0.22 ± 0.12 MPa) (Cunnane et al., 2015). In femoral plaques, failure stress increases from lightly calcified (0.3 ± 0.01 MPa) to moderately calcified plaques (0.43 ± 0.11 MPa) and drastically decreases in heavily calcified plaques (0.16 ± 0.04 MPa). Interestingly, lipid-rich carotid plaques experience a failure stress of 0.342 ± 0.16 MPa, similar to lightly calcified femoral plaques (0.3 ± 0.01 MPa) and heavily calcified carotid plaques with diffuse calcification (0.27 ± 1.73 MPa).

4.5. Summary

The observed global stiffening behaviour of calcified plaques can be attributed to the presence of the calcified deposits, which locally interact with the surrounding tissue matrix. In the majority of reported studies the method of calcification classification is primarily based on semi-quantitative or qualitative techniques, rendering a paucity of detail regarding calcification geometry, location and size. For more precise stiffness estimations, it is important to classify the local tissue behaviour using optical displacement methods, strain distribution through digital image correlation with respect to the calcification features. Plaque strength properties can depend on the calcification geometry and its interaction with the surrounding fibrous tissue matrix. The high degree of variability in failure properties advocates the need to capture local, micron scale fibrous tissue strain distributions in calcified plaques, a requisite for detecting the initiation of plaque rupture (Boekhoven et al., 2014).

5. Modelling for plaque stress assessment

The complexities primarily due to the complicated geometry and material nonlinearity necessitates using computational modelling to assess structural plaque stresses in atherosclerotic plaques under intraluminal blood pressure loading. Hence, the impact of calcifications on plaque stresses is mainly studied by means of finite element modelling (FEM) and fluid solid interaction (FSI) modelling.

5.1. Effect of macro-calcification

An early computational study by (Huang et al., 2001) reported increased peak stresses in plaque specific models when fibrous plaque tissue material properties were assigned to the calcification regions. The change was even more pronounced for larger calcifications, suggesting a stress-reducing effect of calcifications. The same effect was also reported by Vengrenyuk et al. (2008) in a carotid plaque case study, where replacing nodular macro-calcifications at the cap shoulder with fibrous plaque caused an increase in peak stress. In a patient-specific carotid FEM case study, Kiousis et al. (2009) showed reduced plaque stresses if the lipid pool was assigned with calcification material properties. Similarly, Wong

et al. (2012) demonstrated with idealized carotid plaque models a reduction in cap stresses when lipid pool was partially replaced by calcification from the medial side.

Contrary to the above-mentioned studies, suggesting stress-reducing effect of calcifications in atherosclerotic plaques, Teng et al. (2014) reported higher stresses associated with increased total calcification area in a stress analysis study of coronary plaques from ~4500 VH-IVUS frames. The study further demonstrated, after an initial increase, the trend plateaued at a value around ~1.5 mm^2. Similarly, Brown et al. (2016) attributed higher peak stresses in MACE (major adverse cardiovascular event) generating coronary lesions to the presence of larger and more juxtaluminal calcifications in this group, detected by VH-IVUS. Association of higher stresses to juxtaluminal calcifications were also reported by Li et al., (2007) for a small set of idealized (n = 3) and patient-specific (n = 3) carotid plaque models. Similarly, Teng et al. (2014) reported in a patient-specific modelling study of carotid plaques that adding an artificial layer of 200 μm fibrous tissue on the luminal side of superficial calcifications lowered the stresses.

Contrarily, Imoto et al. (2005) demonstrated with idealized FEMs of longitudinal plaque cross-sections that juxtaluminal calcifications located next to a lipid pool lowered cap stresses. Similarly, Hoshino et al. (2009) showed that calcification location with respect to the lipid pool is a determining factor for stress distribution. They used idealized models of rectangular plaque tissue strips with circular rigid and soft inclusions representing calcification and lipid, respectively, exposed to tensile loading. The study also reported that calcification increased plaque stresses at calcification poles facing the tensile loading axis, whereas stresses at the perpendicular poles were reduced.

Teng et al. (2014) reported in their VH-IVUS derived coronary plaque modelling study that the plaque stresses increased with increasing maximum calcification arc and total circumferential length up to ~90–120° and ~25 mm, respectively, and then the trends plateaued. In a computational parametric analysis of idealized coronary plaques, Buffinton and Ebenstein (2014) studied the influence of calcification shape on stresses. The focus was not on the cap region but the calcification-tissue interface as it is a potential stress concentration location due to the stiffness mismatch of the two components. They demonstrated a strong correlation between interface stresses and calcification aspect ratio, where sheet-like (thinner and longer) calcifications had higher interface stresses. The study also demonstrated elevated interface stresses for calcifications with larger area and juxtaluminal location.

5.2. Effect of microcalcification

Mid-2000 s, the hypothesis of increased cap tissue stresses due to the embedded micro-calcifications triggered a new research line. It was first demonstrated, through analytical solution (Vengrenyuk et al., 2006) and later with computational modelling (Rambhia et al., 2012; Vengrenyuk et al. (2006); Bluestein et al., 2008) that micro-calcifications, as stiff inclusions in a relatively more compliant tissue, lead to stress concentrations at the calcification-tissue interface. Subsequent FEM studies not only confirmed a few-fold increase in stress values at the tensile poles of micro-calcifications, but also demonstrated an even greater increase in the case of multiple micro-calcifications in close proximity (Kelly-Arnold et al., 2013; Maldonado et al., 2012). A distance-to-diameter ratio of two micro-calcifications in proximity, smaller than 0.4 amplified the stresses by a factor of five. Moreover, a microcalcification with an elliptical shape was shown to result in greater stresses than a circular shaped one (Vengrenyuk et al., 2008)), especially if it is oriented in the circumferential direction of the plaque cross-section (Cardoso et al., 2014).

A parametric FEM study (Cilla et al., 2013) with idealised geometries of varying cap thickness, and microcalcification size (5–20 μm) and location demonstrated that the cap stress increase due to microcalcification depended on the stress levels of the tissue the microcalcification is embedded in. Stress amplification due to microcalcification presence was reported as minimal if the plaque stresses were already high.

The influence of micro-calcifications on plaque stresses was also investigated through homogenized effective material response approach (Wenk, 2010), where presence of micro-calcifications in a cap sub-region was assumed to result in an overall tissue material behaviour stiffer than the rest of the cap. A shift of peak cap stress towards microcalcification region (Wenk, 2010) and a positive correlation between microcalcification volume fraction and stress increase (Wenk, 2011) were demonstrated. This effect was most noticeable for microcalcification accumulation in the cap shoulder region.

5.3. Calcification stiffness in models and impact on stresses

The variation of material properties applied for the fibrous tissue is a determinant for plaque stresses (Akyildiz et al., 2011). Contrarily, the impact of calcification material properties is accepted to be minimal due to its much greater stiffness compared to other plaque components. In a case study, (Cheng et al., 1993) reported less than 1% change in peak stress when calcification stiffness (~10 MPa) was altered by 900%. (Williamson, 2003) presented less than 10% stress change when the nonlinear constitutive model parameters of calcification varied by 50% Similarly, (Tang et al., 2005) demonstrated less than 10% stress difference when calcification stiffness was changed by 100%. More recently, (Buffinton and Ebenstein, 2014) performed a sensitivity study by varying the calcification stiffness by four orders of magnitude, from 10 MPa to 1 GPa. This wide range was motivated by the authors from the low stiffness measurements of calcified fibrous caps (Loree et al., 1994) and high values measured for plaque calcification with nanoindentation (Ebenstein et al., 2009). Increased calcification stiffness in this wide range resulted in significant rise in the calcification-fibrous tissue interface stresses. However, it is worth to note here that the reported stress values were from the calcification region, not from the plaque tissue.

5.4. Summary

Macrocalcifications can lower the overall stresses in the plaque tissue as their relatively higher stiffness provides them with a greater load bearing capacity. Hence, the mechanical load to be carried by the fibrous tissue and as such stresses in the tissue reduce (Vengrenyuk et al., 2008; Imoto et al., 2005). However, the stress redistribution caused by the presence of a calcification might lead to stress increase in some regions of the plaque tissue as it was reported for the case of juxtaluminally located calcifications (Teng et al., 2014; Li et al., 2007).

Moreover, regardless of the size, calcifications might induce stress concentrations due to the stiffness mismatch with the surrounding plaque tissue, especially in the tensile loading poles of the calcifications (Hoshino et al., 2009). Such local stress concentrations due to micro-calcifications in plaque caps are hypothesized to initiate a tear in plaque tissue, with a chance of further propagation to full-length cap rupture (Cardoso and Weinbaum, 2014). The same hypothesis might also hold for macro-calcifications as plaque fissures extending from macro-calcification-tissue interface to the lumen were reported (Daemen et al., 2016). In case of this scenario, the anisotropic material behaviour of fibrous plaque tissue and the mechanical plaque tissue-calcification interaction are likely determinants of

the interface stress concentrations and possible detachment of the two tissues.

6. Discussion

The search for a parameter that relates the presence of calcification to the likelihood of plaque rupture has been a long arduous clinical research challenge. As indicated in the clinic, deriving a simple correlation between global calcification metrics of area or volume and mechanical stability of plaque is not likely. The true mechanical link between plaque stresses and calcification depends on the various calcification geometric features at multiple length scales and the mechanical factors of the interacting calcification and surrounding fibrous tissue. Hence, it is important to identify (1) what we can learn at micron-scale and how to make use of this information at macroscale, and (2) how we can assess the calcification impact on plaque stability with existing clinical techniques.

6.1. What can be learned from micron scale studies?

Studying the plaques at the fundamental micron and submicron scales is required to provide the essential knowledge base for correct interpretation of the mechanical behaviour that is presented on a macroscale in the clinic. Specifically, the incorporation of the small scale providing intricate details is a biomechanical necessity in order to exploit the diagnostic value of calcification for plaque rupture prediction. Calcification shape, orientation with respect to loading direction, distance and relative location of multiple microcalcifications can induce local stress amplification (Kelly-Arnold et al., 2013). Such stress concentrations are considered to be important for microcalcifications in plaque caps and plaque fissures extending from macrocalcification-tissue interfaces towards the lumen (Daemen et al., 2016). Submicron analysis of the plaque structural morphology by multiphoton, confocal microscopy and micro-CT imaging can be utilised to detect the calcification-tissue interface zones (Gade et al., 2018). Structural alterations in collagen types and individual collagen fiber, and related biomechanical consequences were recently demonstrated for the enthesis tissue of tendons attaching to bone (Rossetti et al., 2017). Similarly, fundamental knowledge of the collagen fiber distribution with respect to the microcalcification particles and macrocalcification geometries will be instrumental to build a knowledge base for utilising calcification related parameters with clinical imaging in the cardiovascular field.

The initiation mechanisms of physiologically induced plaque rupture such as debonding or cavitation, hypothesised by recent computational modelling requires validation (Cardoso and Weinbaum, 2014). A possible way of model validation is comparing the computed model predictions to ex-vivo micro-mechanical testing results (Sang et al., 2018). Local fibre deformation and failure of the calcified plaque can be assessed through micromechanical loading tests coupled with high resolution imaging techniques (Deymier et al., 2017; Rossetti et al., 2017). Remarkably, no experimental evidence has been reported on the failure event, capturing the temporal instability and rupture causality in the plaque caps containing microcalcification particles. Moreover, the reported experimental studies on whole plaques with calcification have advocated a multitude of plaque failure modes by post-failure analysis of the rupture site, including fiber delamination, fiber failure and calcification-fiber interface failures (Barrett et al., 2016; Cunnane et al., 2015; Mulvihill et al., 2013). This underscores the necessity to additionally focus experimental efforts on understanding the interaction properties and forces between calcification and the surrounding fibrous tissue, for example by utilising atomic force microscopy, which can facilitate capturing the forces required to rupture the bond between fibrous tissue and calcification inclusions.

State-of-the-art modelling studies for stress computations mainly treat calcifications as stiff individual inclusions at both micro- and macro-scales. This modelling approach might prove itself clinically useful for macrocalcifications as they can be imaged with clinical techniques. The approach is also of great value to understand possible stress amplification induced by the microcalcifications in the plaque tissue (Cardoso and Weinbaum, 2014). However, it is hard to make it serve for clinical purposes due to limitations of imaging individual micro-calcifications in the clinical setting. Alternatively, as proposed earlier (Wenk, 2011; Wenk, 2010), micro-calcifications can be incorporated in the continuum mechanics based computational models through material response homogenization techniques. These models can be validated, as aforementioned, through macroscale ex-vivo mechanical tests combined with microscale imaging, such as micro-CT to obtain volumetric and distribution data on microcalcifications. If required, more advanced micro-mechanical homogenization models can be developed to incorporate microcalcification size and distance, and capture the calcified plaque tissue material behaviour more accurately. Combined with macrocalcification modelling, this homogenized tissue modelling strategy might provide a clinically relevant computational platform for modelling the coexistence of macro and microcalcifications in plaques.

6.2. How can calcification mechanics be implemented to existing clinical techniques?

Refinements in experiments and computational models in the preclinical setting, incorporating the multiscale nature of the plaque, can be subsequently integrated into the clinic. Non-invasive imaging modalities including CT and MR are currently the most widely used diagnostic approaches in the clinic for the carotid vasculature. With the current technologies it is possible to generate 3D reconstruction of the vessels and resolve macrocalcification geometries as a means to assess their biomechanical impact. Based on patient scan data, studies have generated biomechanical FE models for the computation of plaque-specific stresses (Tang et al., 2017, 2014; Li et al., 2007). Specific geometric configurations can create considerable stress concentrations at the macrocalcification tissue interface which can render the plaque unstable depending on the location of the calcification with respect to the lumen (Buffinton and Ebenstein, 2014). The accuracy of the stress computations is directly a consequence of the image scan quality. The conflicting interference from the high attenuating juxtaluminal calcification and contrast enhanced lumen in CT plaque images makes it difficult to differentiate the surrounding fibrous tissue cap layer. Thus, the ubiquitous ‘stability’ classification for such a plaque scenario must be cautioned when using non-invasive imaging and, in this regard, should provide a means to screen the vessel which can benefit from further invasive imaging assessment. Conversely, the identification of safe ‘stable plaques’ is a promising approach for non-invasive imaging, thereby addressing the patient risk:benefit decision for clinical intervention. For example, with abluminal macrocalcification, while they induce local stress concentrations at the calcification-tissue interface, they can be regarded as low risk as the stress levels experienced at the lumen will largely be minimally affected by the calcification (Wong et al., 2012).

For coronary arteries, invasive imaging techniques (OCT and IVUS) can achieve higher resolution which is instrumental for resolving the juxtaluminal calcification. Juxtaluminally located spotty calcifications (Teng et al., 2014; Li et al., 2007) and orientation of a calcification parallel to a lipid inclusion along the tensile

loading direction were reported to cause stress-elevation (Hoshino et al., 2009). Accuracy of the stress-elevation predictions are largely determined by the accurate reconstruction of plaque morphology from imaging data. Notably, neither modality is optimal for accurate stress predictions. The major disadvantage of IVUS reconstruction is related to resolution capabilities and while OCT overcomes this with superior resolution; however, is hindered by limited penetration constraints. Thus, the fusion of IVUS and OCT can overcome these imaging constraints facilitating whole vessel morphology in addition to accurate fibrous cap thickness (Guo et al., 2017; Molony et al., 2016). In this regard, the co-registration of these two invasive imaging techniques provides advancement for biomechanical modelling with more accuracy for the fibrous cap thickness and local stress–strain computations.

Notably with the aforementioned imaging modalities, we are confined to analysing the macrocalcification as it is not possible to detect the presence of microcalcification particles. Recent hybrid imaging systems, integrating PET with clinical-CT or clinical-MRI, facilitate detecting and differentiating the presence of microcalcification particles and resolving the macrocalcification geometries which is useful for the aforementioned homogenisation approach. The coupling of multiple imaging modalities further permits the acquisition of critical functional information regarding calcified plaque tissue. Patient-specific models can be generated by fusing the three non-invasive modalities (PET, CT and MR) to evaluate fibrous cap's local stress and strain properties (Tang et al., 2017). This will enable adapting a frame-work to assess the mechanical vulnerability associated with presence of microcalcification and macrocalcification in atherosclerotic plaques.

7. Conclusion

In conclusion, the present study was conducted to evaluate the current knowledge base regarding plaque mechanical vulnerability and calcification from a clinical perspective and in parallel with the mechanical evidence derived from ex-vivo experiments and computational simulations. Though the current research has advanced the mechanical understanding of calcification, is it necessary to move our efforts down in scale towards the fundamental micron and submicron scales in order to interpret the true calcified plaques mechanical behaviour that is presented on a macroscale in the clinic.

Conflict of interest

No conflicts of interest to declare.

Acknowledgements

This project has received funding from the European Commission's Horizon 2020 research and innovation programme under the Marie Skłodowska-Curie grant agreement No. 707404 and No. 749283.

References

Agatston, A., Janowitz, W., Hildner, F., Zusmer, N., Viamonte, M., Detrano, R., 1990. Quantification of coronary artery calcium using ultrafast computed tomography. JACC 15, 827–832. https://doi.org/10.1016/0735-1097(90)90282-T.

Aikawa, E., Nahrendorf, M., Figueiredo, J.-L., Swirski, F.K., Shtatland, T., Kohler, R.H., Jaffer, F.a., Aikawa, M., Weissleder, R., 2007. Osteogenesis associates with inflammation in early-stage atherosclerosis evaluated by molecular imaging in vivo. Circulation 116, 2841–2850. https://doi.org/10.1161/CIRCULATIONAHA.107.732867.

Akyildiz, A.C., Chai, C.K., Oomens, C.W.J., van der Lugt, A., Baaijens, F.P.T., Strijkers, G. J., Gijsen, F.J.H., 2017. 3D fiber orientation in atherosclerotic carotid plaques. J. Struct. Biol. 200, 28–35. https://doi.org/10.1016/j.jsb.2017.08.003.

Akyildiz, A.C., Speelman, L., van Brummelen, H., Gutiérrez, M.A., Virmani, R., van der Lugt, A., van der Steen, A.F., Wentzel, J.J., Gijsen, F.J., 2011. Effects of intima stiffness and plaque morphology on peak cap stress. Biomed. Eng. Online 10. https://doi.org/10.1016/j.ehj.2004.01.002.

Bakhshian Nik, A., Hutcheson, J.D., Aikawa, E., 2017. Extracellular vesicles as mediators of cardiovascular calcification. Front. Cardiovasc. Med. 4. https://doi.org/10.3389/fcvm.2017.00078.

Barrett, H.E., Cunnane, E.M., Hidayat, H., O Brien, J.M., Kavanagh, E.G., Walsh, M.T., 2017. Calcification volume reduces stretch capability and predisposes plaque to rupture in an in vitro model of carotid artery stenting. Eur. J. Vasc. Endovasc. Surg. 54, 431–438. https://doi.org/10.1016/j.ejvs.2017.07.022.

Barrett, H.E., Cunnane, E.M., Kavanagh, E.G., Walsh, M.T., 2016. On the effect of calcification volume and configuration on the mechanical behaviour of carotid plaque tissue. J. Mech. Behav. Biomed. Mater. 56, 45–56. https://doi.org/10.1016/j.jmbbm.2015.11.001.

Bertazzo, S., Gentleman, E., Cloyd, K.L., Chester, A.H., Yacoub, M.H., Stevens, M.M., 2013. Nano-analytical electron microscopy reveals fundamental insights into human cardiovascular tissue calcification. Nat. Mater. 12, 576–583. https://doi.org/10.1038/nmat3627.

Bluestein, D., Alemu, Y., Avrahami, I., Gharib, M., Dumont, K., Ricotta, J.J., Einav, S., 2008. Influence of microcalcifications on vulnerable plaque mechanics using FSI modeling. J. Biomech. 41, 1111–1118. https://doi.org/10.1016/j.jbiomech.2007.11.029.

Boekhoven, R.W., Rutten, M.C.M., van Sambeek, M.R., van de Vosse, F.N., Lopata, R.G. P., 2014. Towards mechanical characterization of intact endarterectomy samples of carotid arteries during inflation using Echo-CT. J. Biomech. 47, 805–814. https://doi.org/10.1016/j.jbiomech.2014.01.016.

Boström, K.I., Jiayi, Y., Pierre, J.G., Ana, M.B.-M., Yucheng, Y., 2016. Endothelial-mesenchymal transition in atherosclerotic lesion calcification. Atherosclerosis, 124–127. https://doi.org/10.1186/s40945-017-0033-9.

Boulanger, C.M., Loyer, X., Rautou, P.E., Amabile, N., 2017. Extracellular vesicles in coronary artery disease. Nat. Rev. Cardiol. 14, 259–272. https://doi.org/10.1038/nrcardio.2017.7.

Brown, A.J., Teng, Z., Calvert, P.A., Rajani, N.K., Hennessy, O., Nerlekar, N., Obaid, D.R., Costopoulos, C., Huang, Y., Hoole, S.P., Goddard, M., West, N.E.J., Gillard, J.H., Bennett, M.R., 2016. Plaque structural stress estimations improve prediction of future major adverse cardiovascular events after intracoronary imaging. Circ. Cardiovasc. Imaging 9. https://doi.org/10.1161/CIRCIMAGING.115.004172.

Buffinton, C.M., Ebenstein, D.M., 2014. Effect of calcification modulus and geometry on stress in models of calcified atherosclerotic plaque. Cardiovasc. Eng. Technol. 5, 244–260. https://doi.org/10.1007/s13239-014-0186-6.

Burke, A.P., Weber, D.K., Kolodgie, F.D., Farb, A., Taylor, A.J., Virmani, R., 2001. Pathophysiology of calcium deposition in coronary arteries. Herz 26, 239–244. https://doi.org/10.1007/s00059-001-2293-z.

Cahalane, R.M., Barrett, H.E., O'Brien, J.M., Kavanagh, E.G., Moloney, M.A., Walsh, M. T., 2018. Relating the mechanical properties of atherosclerotic calcification to radiographic density: a nanoindentation approach. Acta Biomater. 80, 228–236. https://doi.org/10.1016/j.actbio.2018.09.010.

Cardoso, L., Kelly-Arnold, A., Maldonado, N., Laudier, D., Weinbaum, S., 2014. Effect of tissue properties, shape and orientation of microcalcifications on vulnerable cap stability using different hyperelastic constitutive models. J. Biomech. 47, 870–877. https://doi.org/10.1016/j.jbiomech.2014.01.010.

Cardoso, L., Weinbaum, S., 2014. Changing views of the biomechanics of vulnerable plaque rupture: a review. Ann. Biomed. Eng. 42, 415–431. https://doi.org/10.1007/s10439-013-0855-x.

Cheng, G., Loree, H., Kamm, R., Fishbein, M., Lee, R., 1993. Distribution of circumferential stress in ruptured and stable atherosclerotic lesions: a structural analysis with histopathological correlation. Circulation 87, 1179–1187. https://doi.org/10.1161/01.CIR.87.4.1179.

Cilla, M., Monterde, D., Peña, E., Martínez, M.Á., 2013. Does microcalcification increase the risk of rupture? Proc. Inst Mech. Eng. Part H J. Eng. Med. 227, 588–599. https://doi.org/10.1177/0954411913479530.

Cnudde, V., Masschaele, B., Dierick, M., Vlassenbroeck, J., Van Hoorebeke, L., Jacobs, P., 2006. Recent progress in X-ray CT as a geosciences tool. Appl. Geochem. 21, 826–832. https://doi.org/10.1016/j.apgeochem.2006.02.010.

Criqui, M.H., Knox, J.B., Denenberg, J.O., Forbang, N.I., McClelland, R.L., Novotny, T.E., Sandfort, V., Waalen, J., Blaha, M.J., Allison, M.A., 2017. Coronary artery calcium volume and density: potential interactions and overall predictive value: the multi-ethnic study of atherosclerosis. JACC Cardiovasc. Imaging 10, 845–854. https://doi.org/10.1016/j.jcmg.2017.04.018.

Cunnane, E.M., Mulvihill, J.J.E., Barrett, H.E., Healy, D.A., Kavanagh, E.G., Walsh, S.R., Walsh, M.T., 2015. Mechanical, biological and structural characterization of human atherosclerotic femoral plaque tissue. Acta Biomater. 11, 295–303. https://doi.org/10.1016/j.actbio.2014.09.024.

Cunnane, E.M., Mulvihill, J.J.E., Barrett, H.E., Hennessy, M.M., Kavanagh, E.G., Walsh, M.T., 2016. Mechanical properties and composition of carotid and femoral atherosclerotic plaques: a comparative study. J. Biomech. 49, 3697–3704. https://doi.org/10.1016/j.jbiomech.2016.09.036.

Daemen, M.J., Ferguson, M.S., Gijsen, F.J., Hippe, D.S., Kooi, M.E., Demarco, K., van der Wal, A.C., Yuan, C., Hatsukami, T.S., 2016. Carotid plaque fissure: an underestimated source of intraplaque hemorrhage. Atherosclerosis 254, 102–108. https://doi.org/10.1016/j.atherosclerosis.2016.09.069.

Den Hartog, A.G., Bovens, S.M., Koning, W., Hendrikse, J., Luijten, P.R., Moll, F.L., Pasterkamp, G., De Borst, G.J., 2013. Current status of clinical magnetic resonance imaging for plaque characterisation in patients with carotid artery

stenosis. Eur. J. Vasc. Endovasc. Surg. 45, 7–21. https://doi.org/10.1016/j.ejvs.2012.10.022.
Deymier, A.C., An, Y., Boyle, J.J., Schwartz, A.G., Birman, V., Genin, G.M., Thomopoulos, S., Barber, A.H., 2017. Micro-mechanical properties of the tendon-to-bone attachment. Acta Biomater. 56, 25–35. https://doi.org/10.1016/j.actbio.2017.01.037.
Doris, M.K., Newby, D.E., 2016. Identification of early vascular calcification with18F-sodium fluoride: potential clinical application. Exp. Rev. Cardiovasc. Ther. 14, 691–701. https://doi.org/10.1586/14779072.2016.1151354.
Dweck, M.R., Aikawa, E., Newby, D.E., Tarkin, J.M., Rudd, J.H.F., Narula, J., Fayad, Z.A., 2016. Noninvasive molecular imaging of disease activity in atherosclerosis. Circ. Res. 119, 330–340. https://doi.org/10.1161/CIRCRESAHA.116.307971.
Ebenstein, D.M., Coughlin, D., Chapman, J., Li, C., Pruitt, L.A., 2009. Nanomechanical properties of calcification, fibrous tissue, and hematoma from atherosclerotic plaques. J. Biomed. Mater. Res. – Part A 91, 1028–1037. https://doi.org/10.1002/jbm.a.32321.
Friedrich, G.J., Moes, N.Y., Mühlberger, V.a., Gabl, C., Mikuz, G., Hausmann, D., Fitzgerald, P.J., Yock, P.G., 1994. Detection of intralesional calcium by intracoronary ultrasound depends on the histologic pattern. Am. Heart J. 128, 435–441. https://doi.org/10.1016/0002-8703(94)90614-9.
Fujimoto, J.G., 2003. Optical coherence tomography for ultrahigh resolution in vivo imaging. Nat. Biotechnol. 21, 1361–1367. https://doi.org/10.1038/nbt892.
Gade, P.S., Robertson, A.M., Chuang, C.-Y., 2018. Multiphoton imaging of collagen, elastin, and calcification in intact soft-tissue samples. Curr. Protoc. Cytom. https://doi.org/10.1002/cpcy.51 e51.
Greenland, P., Blaha, M.J., Budoff, M.J., Erbel, R., Watson, K.E., 2018. Coronary calcium score and cardiovascular risk. J. Am. Coll. Cardiol. 72, 434–447. https://doi.org/10.1016/j.jacc.2018.05.027.
Guihard, P.J., Yao, J., Blazquez-Medela, A.M., Iruela-Arispe, L., Boström, K.I., Yao, Y., 2016. Endothelial-mesenchymal transition in vascular calcification of Ins2Akita/+ Mice. PLoS One 11, 1–12. https://doi.org/10.1371/journal.pone.0167936.
Guo, X., Giddens, D.P., Molony, D., Yang, C., Samady, H., Zheng, J., Mintz, G., Maehara, A., Wang, L., Pei, X., Li, Z.-Y., Tang, D., 2017. An FSI modeling approach to combine IVUS and OCT for more accurate patient-specific coronary cap thickness and stress/strain calculations. J. Biomech. Eng. 10 (1115/1), 4038263.
Gupta, A., Mtui, E.E., Baradaran, H., Salama, G., Pandya, A., Kamel, H., Giambrone, A., Sanelli, P.C., 2015. CT angiographic features of symptom-producing plaque in moderate-grade carotid artery stenosis. Am. J. Neuroradiol. 36, 349–354. https://doi.org/10.3174/ajnr.A4098.
Herisson, F., Heymann, M.F., Chétiveaux, M., Charrier, C., Battaglia, S., Pilet, P., Rouillon, T., Krempf, M., Lemarchand, P., Heymann, D., Gouëffic, Y., 2011. Carotid and femoral atherosclerotic plaques show different morphology. Atherosclerosis 216, 348–354. https://doi.org/10.1016/j.atherosclerosis.2011.02.004.
Holzapfel, G.A., Sommer, G., Regitnig, P., 2004. Anisotropic mechanical properties of tissue components in human atherosclerotic plaques. J. Biomech. Eng. 126, 657. https://doi.org/10.1016/0025-5408(88)90092-X.
Hoshino, T., Chow, L.A., Hsu, J.J., Perlowski, A.A., Abedin, M., Tobis, J., Tintut, Y., Mal, A.K., Klug, W.S., Demer, L.L., 2009. Mechanical stress analysis of a rigid inclusion in distensible material: a model of atherosclerotic calcification and plaque vulnerability. Am. J. Physiol. Circ. Physiol. 297, H802–H810. https://doi.org/10.1152/ajpheart.00318.2009.
Huang, H., Virmani, R., Younis, H., Burke, A.P., Kamm, R.D., Lee, R.T., 2001. The impact of calcification on the biomechanical stability of atherosclerotic plaques. Circulation 103, 1051–1056.
Hunt, J.L., Fairman, R., Mitchell, M.E., Carpenter, J.P., Golden, M., Khalapyan, T., Wolfe, M., Neschis, D., Milner, R., Scoll, B., Cusack, A., Mohler, E.R., 2002. Bone formation in carotid plaques: a clinicopathological study. Stroke 33, 1214–1219. https://doi.org/10.1161/01.STR.0000013741.41309.67.
Hutcheson, J.D., Goettsch, C., Bertazzo, S., Maldonado, N., Ruiz, J.L., Goh, W., Yabusaki, K., Faits, T., Bouten, C., Franck, G., Quillard, T., Libby, P., Aikawa, M., Weinbaum, S., Aikawa, E., 2016. Genesis and growth of extracellular-vesicle-derived microcalcification in atherosclerotic plaques. Nat. Mater. 15, 335–343. https://doi.org/10.1038/nmat4519.
Imoto, K., Hiro, T., Fujii, T., Murashige, A., Fukumoto, Y., Hashimoto, G., Okamura, T., Yamada, J., Mori, K., Matsuzaki, M., 2005. Longitudinal structural determinants of atherosclerotic plaque vulnerability: a computational analysis of stress distribution using vessel models and three-dimensional intravascular ultrasound imaging. J. Am. Coll. Cardiol. 46, 1507–1515. https://doi.org/10.1016/j.jacc.2005.06.069.
Irkle, A., Vesey, A.T., Lewis, D.Y., Skepper, J.N., Bird, J.L.E., Dweck, M.R., Joshi, F.R., Gallagher, F.A., Warburton, E.A., Bennett, M.R., Brindle, K.M., Newby, D.E., Rudd, J.H., Davenport, A.P., 2015. Identifying active vascular microcalcification by ^{18}F-sodium fluoride positron emission tomography. Nat. Commun. 6. https://doi.org/10.1038/ncomms8495.
Jia, H., Abtahian, F., Aguirre, A.D., Lee, S., Chia, S., Lowe, H., Kato, K., Yonetsu, T., Vergallo, R., Hu, S., Tian, J., Lee, H., Park, S.J., Jang, Y.S., Raffel, O.C., Mizuno, K., Uemura, S., Itoh, T., Kakuta, T., Choi, S.Y., Dauerman, H.L., Prasad, A., Toma, C., McNulty, I., Zhang, S., Yu, B., Fuster, V., Narula, J., Virmani, R., Jang, I.K., 2013. In vivo diagnosis of plaque erosion and calcified nodule in patients with acute coronary syndrome by intravascular optical coherence tomography. J. Am. Coll. Cardiol. 62, 1748–1758. https://doi.org/10.1016/j.jacc.2013.05.071.
Jian, X., Han, Z., Liu, P., Xu, J., Li, Z., Li, P., Shao, W., Cui, Y., 2017. A High frequency geometric focusing transducer based on 1–3 piezocomposite for intravascular ultrasound imaging. Biomed Res. Int. 2017. https://doi.org/10.1155/2017/9327270.
Johnson, R.C., Leopold, J.A., Loscalzo, J., 2006. Vascular calcification: pathobiological mechanisms and clinical implications. Circ. Res. 99, 1044–1059. https://doi.org/10.1161/01.RES.0000249379.55535.21.
Kataoka, Y., Puri, R., Hammadah, M., Duggal, B., Uno, K., Kapadia, S.R., Tuzcu, E.M., Nissen, S.E., Nicholls, S.J., Tuzcu, M., Nissen, S.E., Nicholls, S.J., 2014. Spotty calcification and plaque vulnerability in vivo : frequency-domain optical coherence tomography analysis. Cardiovasc. Diagn. Ther. 4, 460–469. https://doi.org/10.3978/j.issn.2223-3652.2014.11.06.
Kelly-Arnold, A., Maldonado, N., Laudier, D., Aikawa, E., Cardoso, L., Weinbaum, S., 2013. Revised microcalcification hypothesis for fibrous cap rupture in human coronary arteries. Proc. Natl. Acad. Sci. 110, 10741–10746. https://doi.org/10.1073/pnas.1308814110.
Kiousis, D.E., Rubinigg, S.F., Auer, M., Holzapfel, G.A., 2009. A methodology to analyze changes in lipid core and calcification onto fibrous cap vulnerability: the human atherosclerotic carotid bifurcation as an illustratory example. J. Biomech. Eng. 131,. https://doi.org/10.1115/1.4000078 121002.
Kwee, R.M., 2010. Systematic review on the association between calcification in carotid plaques and clinical ischemic symptoms. J. Vasc. Surg. 51, 1015–1025. https://doi.org/10.1016/j.jvs.2009.08.072.
Lawlor, M.G., O'Donnell, M.R., O'Connell, B.M., Walsh, M.T., 2011. Experimental determination of circumferential properties of fresh carotid artery plaques. J. Biomech. 44, 1709–1715. https://doi.org/10.1016/j.jbiomech.2011.03.033.
Leszczynska, A., O'Doherty, A., Farrell, E., Pindjakova, J., O'Brien, F.J., O'Brien, T., Barry, F., Murphy, M., 2016. Differentiation of vascular stem cells contributes to ectopic calcification of atherosclerotic plaque. Stem Cells 34, 913–923. https://doi.org/10.1002/stem.2315.
Li, Z.Y., Howarth, S., Tang, T., Graves, M., U-King-Im, J., Gillard, J.H., 2007. Does calcium deposition play a role in the stability of atheroma? Location may be the key. Cerebrovasc. Dis. 24, 452–459. https://doi.org/10.1159/000108436.
Loree, H.M., Tobias, B.J., Gibson, L.J., Kamm, R.D., Small, D.M., Lee, R.T., 1994. Mechanical properties of model atherosclerotic lesion lipid pools. Arterioscler. Thromb. 14, 230–234. https://doi.org/10.1161/01.ATV.14.2.230.
Maher, E., Creane, A., Sultan, S., Hynes, N., Lally, C., Kelly, D.J., 2009. Tensile and compressive properties of fresh human carotid atherosclerotic plaques. J Biomech 42, 2760–2767.
Maher, E., Creane, A., Sultan, S., Hynes, N., Lally, C., Kelly, D.J., 2011. Inelasticity of human carotid atherosclerotic plaque. Ann. Biomed. Eng. 39, 2445–2455. https://doi.org/10.1007/s10439-011-0331-4.
Maldonado, N., Kelly-Arnold, A., Vengrenyuk, Y., Laudier, D., Fallon, J.T., Virmani, R., Cardoso, L., Weinbaum, S., 2012. A mechanistic analysis of the role of microcalcifications in atherosclerotic plaque stability: potential implications for plaque rupture. Am. J. Physiol. Circ. Physiol. 303, H619–H628. https://doi.org/10.1152/ajpheart.00036.2012.
Mehenna, E., Bezerra, H., Prabhu, D., Brandt, E., Chamié, D., Yamamoto, H., Attizzani, G.F., Tahara, S., Van Ditzhuijzen, N., Fujino, Y., Kanaya, T., Stefano, G., Mehanna, E., Bezerra, H.G., Prabhu, D., Brandt, E., Chamie, D., Van Ditzhuijzen, N., Wang, W., Gargesha, M., Wilson, D., Costa, M.a., Chamié, D., Yamamoto, H., Attizzani, G. F., Tahara, S., Van Ditzhuijzen, N., Fujino, Y., Kanaya, T., Stefano, G., Wang, W., Gargesha, M., Wilson, D., Costa, M.a., 2013. Volumetric characterization of human coronary calcification by frequency-domain optical coherence tomography. Circ. J. 77, 2334–2340. https://doi.org/10.1253/circj.CJ-12-1458.
Menini, S., Iacobini, C., Ricci, C., Fantauzzi, C.B., Salvi, L., Pesce, C.M., Relucenti, M., Familiari, G., Taurino, M., Pugliese, G., 2013. The galectin-3/RAGE dyad modulates vascular osteogenesis in atherosclerosis. Cardiovasc. Res. 100, 472–480. https://doi.org/10.1093/cvr/cvt206.
Molony, D.S., Timmins, L.H., Rasoul-Arzrumly, E., Samady, H., Giddens, D.P., 2016. Evaluation of a framework for the co-registration of intravascular ultrasound and optical coherence tomography coronary artery pullbacks. J. Biomech. 49, 4048–4056. https://doi.org/10.1016/j.jbiomech.2016.10.040.
Mulvihill, J.J., Cunnane, E.M., McHugh, S.M., Kavanagh, E.G., Walsh, S.R., Walsh, M.T., 2013. Mechanical, biological and structural characterization of in vitro ruptured human carotid plaque tissue. Acta Biomater. 9, 9027–9035. https://doi.org/10.1016/j.actbio.2013.07.012.
Nerlekar, N., Ha, F.J., Cheshire, C., Rashid, H., Cameron, J.D., Wong, D.T., Seneviratne, S., Brown, A.J., 2018. Computed tomographic coronary angiography-derived plaque characteristics predict major adverse cardiovascular events clinical perspective. Circ. Cardiovasc. Imaging 11,. https://doi.org/10.1161/CIRCIMAGING.117.006973 e006973.
New, S.E.P., Goettsch, C., Aikawa, M., Marchini, J.F., Shibasaki, M., Yabusaki, K., Libby, P., Shanahan, C.M., Croce, K., Aikawa, E., 2013. Macrophage-derived matrix vesicles: an alternative novel mechanism for microcalcification in atherosclerotic plaques. Circ. Res. 113, 72–77. https://doi.org/10.1161/CIRCRESAHA.113.301036.
Nikolaou, K., Flohr, T., Knez, A., Rist, C., Wintersperger, B., Johnson, T., Reiser1, M.F., Becker, C.R., 2004. Advances in cardiac CT imaging: 64-slice scanner. Int. J. Cardiovasc. Imaging 20, 535–540. https://doi.org/10.3109/01612840.2016.1162882.
Perrotta, I., Perri, E., 2017. Ultrastructural, elemental and mineralogical analysis of vascular calcification in atherosclerosis. Microsc. Microanal. 23, 1030–1039. https://doi.org/10.1017/S1431927617012533.
Puppini, G., Furlan, F., Cirota, N., Veraldi, G., Piubello, Q., Montemezzi, S., Gortenuti, G., 2006. Caratterizzazione delle placche carotidee aterosclerotiche: comparazione tra risonanza magnetica e istologia. Radiol. Medica 111, 921–930. https://doi.org/10.1007/s11547-006-0091-7.

Raggi, P., Genest, J., Giles, J.T., Rayner, K.J., Dwivedi, G., Beanlands, R.S., Gupta, M., 2018. Role of inflammation in the pathogenesis of atherosclerosis and therapeutic interventions. Atherosclerosis 276, 98–108. https://doi.org/10.1016/j.atherosclerosis.2018.07.014.

Rambhia, S.H., Liang, X., Xenos, M., Alemu, Y., Maldonado, N., Kelly, A., Chakraborti, S., Weinbaum, S., Cardoso, L., Einav, S., Bluestein, D., 2012. Microcalcifications increase coronary vulnerable plaque rupture potential: a patient-based micro-CT fluid-structure interaction study. Ann. Biomed. Eng. 40, 1443–1454. https://doi.org/10.1007/s10439-012-0511-x.

Richardson, P.D., 2002. Biomechanics of plaque rupture: progress, problems, and new frontiers. Ann. Biomed. Eng. 30, 524–536. https://doi.org/10.1114/1.1482781.

Robson, P.M., Dweck, M.R., Trivieri, M.G., Karakatsanis, N.A., Contreras, J., Gidwani, U., Narula, J.P., Fuster, V., Kovacic, J.C., Fayad, A., Kingdom, U., 2018. Coronary artery PET/MR imaging: feasibility, limitations, and solutions. JACC Cardiovasc. Imaging 10, 1103–1112. https://doi.org/10.1016/j.jcmg.2016.09.029.Coronary.

Rossetti, L., Kuntz, L.A., Kunold, E., Schock, J., Müller, K.W., Grabmayr, H., Stolberg-Stolberg, J., Pfeiffer, F., Sieber, S.A., Burgkart, R., Bausch, A.R., 2017. The microstructure and micromechanics of the tendon-bone insertion. Nat. Mater. 16, 664–670. https://doi.org/10.1038/nmat4863.

Saam, T., Hatsukami, T.S., Underhill, H., Kerwin, W.S., Ferguson, M.S., 2007. Atherosclerotic plaque: noninvasive MR imaging for. Radiology 244.

Sakaguchi, M., Hasegawa, T., Ehara, S., Matsumoto, K., Mizutani, K., Iguchi, T., Ishii, H., Nakagawa, M., Shimada, K., Yoshiyama, M., 2016. New insights into spotty calcification and plaque rupture in acute coronary syndrome: an optical coherence tomography study. Heart Vessels 31, 1915–1922. https://doi.org/10.1007/s00380-016-0820-3.

Salunke, N., Topoleski, L.D., Humphrey, J., Mergner, W., 2001. Compressive stress-relaxation of human atherosclerotic plaque. J. Biomed. Mater. Res. 55, 236–241. https://doi.org/10.1002/1097-4636(200105)55:2<236::AID-JBM1010>3.0.CO;2-F.

Sánchez-Duffhues, G., De Vinuesa, A.G., Lindeman, J.H., Mulder-Stapel, A., DeRuiter, M.C., Van Munsteren, C., Goumans, M.J., Hierck, B.P., Ten Dijke, P., 2015. SLUG is expressed in endothelial cells lacking primary cilia to promote cellular calcification. Arterioscler. Thromb. Vasc. Biol. 35, 616–627. https://doi.org/10.1161/ATVBAHA.115.305268.

Sang, C., Maiti, S., Fortunato, R.N., Kofler, J., Robertson, A.M., 2018. A uniaxial testing approach for consistent failure in vascular tissues. J. Biomech. Eng. 140, 61010.

Sarwar, A., Rieber, J., Mooyaart, E.A., Seneviratne, S.K., Houser, S.L., Bamberg, F., Raffel, O.C., Gupta, R., Kalra, M.K., Pien, H., Lee, H., 2008. Calcified plaque: measurement of area at thin-section flat-panel CT and 64-section multidetector CT and comparison with histopathologic findings. Radiology 249 (1), 301–306.

Shanahan, C.M., 2007. Inflammation ushers in calcification: a cycle of damage and protection? Circulation 116, 2782–2785. https://doi.org/10.1161/CIRCULATIONAHA.107.749655.

Spagnoli, L.G., Mauriello, A., Sangiorgi, G., Fratoni, S., Bonanno, E., Schwartz, R.S., Piepgras, D.G., Pistolese, R., Ippoliti, A., 2004. Carotid plaque as a risk factor for ischemic stroke. J. Am. Med. Assoc. 292, 1845–1852. https://doi.org/10.1001/jama.292.15.1845.

Stary, H.C., 2000. Natural history of calcium deposits in atherosclerosis progression and regression. Zeitschrift für Kardiologie 89 (14), S028–S35. https://doi.org/10.1007/s003920070097.

Tang, D., Yang, C., Huang, S., Mani, V., Zheng, J., Woodard, P.K., Robson, P., Teng, Z., Dweck, M., Fayad, Z.A., 2017. Cap inflammation leads to higher plaque cap strain and lower cap stress: an MRI-PET/CT-based FSI modeling approach. J. Biomech. 50, 121–129. https://doi.org/10.1016/j.jbiomech.2016.11.011.

Tang, D., Yang, C., Zheng, J., Woodard, P.K., Saffitz, J.E., Sicard, G.A., Pilgram, T.K., Yuan, C., 2005. Quantifying effects of plaque structure and material properties on stress distributions in human atherosclerotic plaques using 3D FSI models. J. Biomech. Eng. 127, 1185. https://doi.org/10.1115/1.2073668.

Tearney, G.J., Regar, E., Akasaka, T., Adriaenssens, T., Barlis, P., Bezerra, H.G., Bouma, B., Bruining, N., Cho, J.M., Chowdhary, S., Costa, M.A., De Silva, R., Dijkstra, J., Di Mario, C., Dudeck, D., Falk, E., Feldman, M.D., Fitzgerald, P., Garcia, H., Gonzalo, N., Granada, J.F., Guagliumi, G., Holm, N.R., Honda, Y., Ikeno, F., Kawasaki, M., Kochman, J., Koltowski, L., Kubo, T., Kume, T., Kyono, H., Lam, C.C.S., Lamouche, G., Lee, D.P., Leon, M.B., Maehara, A., Manfrini, O., Mintz, G.S., Mizuno, K., Morel, M.A., Nadkarni, S., Okura, H., Otake, H., Pietrasik, A., Prati, F., Rber, L., Radu, M.D., Rieber, J., Riga, M., Rollins, A., Rosenberg, M., Sirbu, V., Serruys, P.W.J.C., Shimada, K., Shinke, T., Shite, J., Siegel, E., Sonada, S., Suter, M., Takarada, S., Tanaka, A., Terashima, M., Troels, T., Uemura, S., Ughi, G.J., Van Beusekom, H.M. M., Van Der Steen, A.F.W., Van Es, G.A., Van Soest, G., Virmani, R., Waxman, S., Weissman, N.J., Weisz, G., 2012. Consensus standards for acquisition, measurement, and reporting of intravascular optical coherence tomography studies: a report from the International Working Group for Intravascular Optical Coherence Tomography Standardization and Validation. J. Am. Coll. Cardiol. 59, 1058–1072. https://doi.org/10.1016/j.jacc.2011.09.079.

Teng, Z., Brown, A.J., Calvert, P.A., Parker, R.A., Obaid, D.R., Huang, Y., Hoole, S.P., West, N.E.J., Gillard, J.H., Bennett, M.R., 2014. Coronary plaque structural stress is associated with plaque composition and subtype and higher in acute coronary syndrome: the BEACON I (Biomechanical Evaluation of Atheromatous Coronary Arteries) study. Circ. Cardiovasc. Imaging 7, 461–470. https://doi.org/10.1161/CIRCIMAGING.113.001526.

Teng, Z., He, J., Sadat, U., Mercer, J.R., Wang, X., Bahaei, N.S., Thomas, O.M., Gillard, J. H., 2014. How does juxtaluminal calcium affect critical mechanical conditions in carotid atherosclerotic plaque? An exploratory study. IEEE Trans. Biomed. Eng. 61, 35–40. https://doi.org/10.1109/TBME.2013.2275078.

van Der Giessen, A.G., Gijsen, F.J.H., Wentzel, J.J., Jairam, P.M., Van Walsum, T., Neefjes, L.A.E., Mollet, N.R., Niessen, W.J., Van De Vosse, F.N., De Feyter, P.J., Van Der Steen, A.F.W., 2011. Small coronary calcifications are not detectable by 64-slice contrast enhanced computed tomography. Int. J. Cardiovasc. Imaging 27, 143–152. https://doi.org/10.1007/s10554-010-9662-8.

van Wijk, D.F., Strang, A.C., Duivenvoorden, R., Enklaar, D.J.F., Zwinderman, A.H., Van Der Geest, R.J., Kastelein, J.J.P., De Groot, E., Stroes, E.S.G., Nederveen, A.J., 2015. Increasing the spatial resolution of 3T carotid MRI has no beneficial effect for plaque component measurement reproducibility. PLoS One 10, 1–15. https://doi.org/10.1371/journal.pone.0130878.

Vengrenyuk, Y., Cardoso, L., Weinbaum, S., 2008. Micro-CT based analysis of a new paradigm for vulnerable plaque rupture: cellular microcalcifications in fibrous caps. MCB Mol. Cell. Biomech. 5, 37–47. https://doi.org/10.3970/mcb.2008.005.037.

Vengrenyuk, Y., Carlier, S., Xanthos, S., Cardoso, L., Ganatos, P., Virmani, R., Einav, S., Gilchrist, L., Weinbaum, S., 2006. A hypothesis for vulnerable plaque rupture due to stress-induced debonding around cellular microcalcifications in thin fibrous caps. Proc. Natl. Acad. Sci. 103, 14678–14683. https://doi.org/10.1073/pnas.0606310103.

Vesey, A.T., Jenkins, W.S.A., Irkle, A., Moss, A., Sng, G., Forsythe, R.O., Clark, T., Roberts, G., Fletcher, A., Lucatelli, C., Rudd, J.H.F., Davenport, A.P., Mills, N.L., Al-Shahi Salman, R., Dennis, M., Whiteley, W.N., Van Beek, E.J.R., Dweck, M.R., Newby, D.E., 2017. 18F-fluoride and18F-fluorodeoxyglucose positron emission tomography after transient ischemic attack or minor ischemic stroke: case-control study. Circ. Cardiovasc. Imaging 10. https://doi.org/10.1161/CIRCIMAGING.116.004976.

Virmani, R., Burke, A.P., Farb, A., Kolodgie, F.D., 2006. Pathology of the vulnerable plaque. J. Am. Coll. Cardiol. 47, 7–12. https://doi.org/10.1016/j.jacc.2005.10.065.

Wenk, J.F., 2010. Numerical modeling of stress in stenotic arteries with microcalcifications: a micromechanical approximation. J. Biomech. Eng. 132,. https://doi.org/10.1115/1.4001351 091011.

Wenk, J.F., 2011. Numerical modeling of stress in stenotic arteries with microcalcifications: a parameter sensitivity study. J. Biomech. Eng. 133, 14503. https://doi.org/10.1115/1.4003128.

Williamson, S.D., 2003. On the sensitivity of wall stresses in diseased arteries to variable material properties. J. Biomech. Eng. 125, 147. https://doi.org/10.1115/1.1537736.

Wong, K.K.L., Thavornpattanapong, P., Cheung, S.C.P., Sun, Z., Tu, J., 2012. Effect of calcification on the mechanical stability of plaque based on a three-dimensional carotid bifurcation model. BMC Cardiovasc. Disord. 12, 7. https://doi.org/10.1186/1471-2261-12-7.

Yahagi, K., Davis, H.R., Arbustini, E., Virmani, R., 2015. Sex differences in coronary artery disease: pathological observations. Atherosclerosis 239, 260–267. https://doi.org/10.1016/j.atherosclerosis.2015.01.017.

Yang, J., Pan, X., Zhang, B., Yan, Y., Huang, Y., Woolf, A., Gillard, J., Teng, Z., Hui, P., 2018. Superficial and multiple calcifications and ulceration associate with intraplaque hemorrhage in the carotid atherosclerotic plaque. Eur. Radiol. 1–10. https://doi.org/10.1007/s00330-018-5535-7.

Yao, Y., Jumabay, M., Ly, A., Radparvar, M., Cubberly, M.R., Boström, K.I., 2013. A role for the endothelium in vascular calcification. Circ. Res. 113, 495–504. https://doi.org/10.1161/CIRCRESAHA.113.301792.